The Star Formation History and Dynamics of the Ultra-diffuse Galaxy Dragonfly 44 in MOND and MOG

Hosein Haghi[1] , Vahid Amiri[1], Akram Hasani Zonoozi[1,2] , Indranil Banik[2] , Pavel Kroupa[2,3] , and Moritz Haslbauer[2]
[1] Department of Physics, Institute for Advanced Studies in Basic Sciences (IASBS), P.O. Box 11365-9161, Zanjan, Iran; haghi@iasbs.ac.ir
[2] Helmholtz-Institut für Strahlen-und Kernphysik (HISKP), Universität Bonn, Nussallee 14-16, D-53115 Bonn, Germany
[3] Charles University in Prague, Faculty of Mathematics and Physics, Astronomical Institute, V Holešovičkách 2, CZ-180 00, Praha 8, Czech Republic

Abstract

The observed line-of-sight velocity dispersion $\sigma_{\rm los}$ of the ultra-diffuse galaxy Dragonfly 44 (DF44) requires a Newtonian dynamical mass-to-light ratio of $M_{\rm dyn}/L_I = 26^{+7}_{-6}$ solar units. This is well outside the acceptable limits of our stellar population synthesis (SPS) models, which we construct using the integrated galactic initial mass function (IGIMF) theory. Assuming DF44 is in isolation and using Jeans analysis, we calculate $\sigma_{\rm los}$ profiles of DF44 in Milgromian dynamics (MOND) and modified gravity (MOG) theories without invoking dark matter. Comparing with the observed kinematics, the best-fitting MOND model has $M_{\rm dyn}/L_I = 3.6^{+1.6}_{-1.2}$ and a constant orbital anisotropy of $\beta = -0.5^{+0.4}_{-1.6}$. In MOG, we first fix its two theoretical parameters α and μ based on previous fits to the observed rotation curve data of The HI Nearby Galaxy Survey (THINGS). The DF44 $\sigma_{\rm los}$ profile is best fit with $M_{\rm dyn}/L_I = 7.4^{+1.5}_{-1.4}$, larger than plausible SPS values. MOG produces a $\sigma_{\rm los}$ profile for DF44 with acceptable $M_{\rm dyn}/L_I$ and isotropic orbits if α and μ are allowed to vary. MOND with the canonical a_0 can explain DF44 at the 2.40σ confidence level (1.66%) if considering both its observed kinematics and typical star formation histories in an IGIMF context. However, MOG is ruled out at 5.49σ (P-value of 4.07×10^{-8}) if its free parameters are fixed at the highest values consistent with THINGS data.

Unified Astronomy Thesaurus concepts: Gravitation (661); Modified Newtonian dynamics (1069); Dwarf galaxies (416); Galaxy dynamics (591)

1. Introduction

Ultra-diffuse galaxies (UDGs; van Dokkum et al. 2015) are characterized by an extremely low surface brightness of $\mu_{(g,0)} < 24$ mag arcsec^{-2}, comparable to those of dwarf galaxies. But unlike dwarfs, UDGs have extended stellar distributions, sometimes with a size comparable to that of the Milky Way ($\approx$4 kpc).

van Dokkum et al. (2018) and van Dokkum et al. (2019a) previously reported the discovery of two "dark-matter-free" UDGs, NGC 1052-DF2 (DF2) and NGC 1052-DF4 (DF4), with line-of-sight velocity dispersions of $\sigma_{\rm los} = 8.5^{+2.2}_{-3.1}$ km s^{-1} (Danieli et al. 2019) and $\sigma_{\rm los} = 4.2^{+4.4}_{-2.2}$ km s^{-1} (van Dokkum et al. 2019b), respectively. In both cases, the upper limit to the halo mass is $M_{200} \lesssim 10^8 M_\odot$ (van Dokkum et al. 2018, 2019a; Wasserman et al. 2018). They argue that the apparent lack of dark matter in DF2 and DF4 is in contrast to Dragonfly 44 (DF44), which is gravitationally dominated by dark matter (van Dokkum et al. 2016). This large apparent difference in dark matter content is surprising as DF2, DF4, and DF44 have very similar stellar mass and morphology.

UDGs are also interesting systems for testing classical and alternative gravity theories such as Milgrom's modified Newtonian dynamics (MOND; Milgrom 1983a) or Moffat's modified gravity (MOG; Moffat 2005). UDGs generally experience internal accelerations below the characteristic MOND acceleration of $a_0 = 1.2 \times 10^{-10}$ m s^{-2}. Therefore, MOND predicts a different $\sigma_{\rm los}$ than Newtonian dynamics in the absence of dark matter. In Kroupa et al. (2018) and Haghi et al. (2019), we calculated $\sigma_{\rm los}$ for the UDGs DF2 and DF4 using a new analytic formulation and fully self-consistent live N-body models in MOND. We showed that the velocity dispersion calculated by taking into account the external field

effect (EFE) from possible host galaxies leads to $\sigma_{\rm los}$ being well consistent with the observed values in both cases. The same conclusions are reached independently by Famaey et al. (2018).

The velocity dispersion profile of UDGs can also be modeled using the appropriate Jeans equation, from which one can derive the statistical properties of the velocity distribution of stars (Binney & Tremaine 2008). This calculation requires knowledge of the gravitational potential and the stellar density distribution, in addition to some assumptions about the shape of the velocity distribution.

Taking $\sigma_{\rm los}$ to be a function of radius alone for eight MW dwarf spheroidal galaxies (dSphs) and using spherical Jeans analysis, Angus & McGaugh (2008) showed that most of them have a MOND dynamical $M_{\rm dyn}/L$ ratio compatible with stellar population synthesis (SPS) models. Using Jeans analysis, Haghi & Amiri (2016) studied the internal dynamics of eight MW dSphs in the framework of the MOG theory. They showed that when letting the two MOG parameters α and μ (Section 3.1) vary on a case by case basis, the best-fitted $M_{\rm dyn}/L$ ratios for almost all dSphs are comparable with the SPS values. However, this eliminates the predictability of the theory.

In this contribution, we focus on DF44, a UDG in the Coma Cluster (van Dokkum et al. 2016; Di Cintio et al. 2017). Recently, van Dokkum et al. (2019b) obtained a revised mean line-of-sight velocity dispersion within its half-light radius of $\sigma_{\rm los} = 33$ km s^{-1} and thus an estimated halo mass of $M_{200} = 10^{11}$–$10^{12} M_\odot$. DF44 has a rising $\sigma_{\rm los}$ profile, from $\sigma_{\rm los} = 26 \pm 4$ km s^{-1} at $R = 0.2$ kpc to $\sigma_{\rm los} = 41 \pm 8$ km s^{-1} at $R = 5.1$ kpc, with no observed signs of rotation. They showed that this profile can only be fit with a standard Navarro–Frenk–White halo if the velocity distribution has a

strong tangential anisotropy ($\beta = -0.8^{+0.4}_{-0.5}$). A good fit also results from a dark matter halo with a relatively flat density profile (e.g., Di Cintio et al. 2014) and no orbital anisotropy ($\beta = -0.1^{+0.2}_{-0.3}$). van Dokkum et al. (2019b) also calculated the mass profile of DF44, finding a Newtonian dynamical mass-to-light ratio (M/L) in the photometric I–band of $M_{\rm dyn}/L_I = 26^{+7}_{-6}$ solar units within the effective radius of ≈ 3 kpc. The reported $M_{\rm dyn}/L_I$ is similar to other UDGs but $\approx 6\times$ higher than normal galaxies of the same luminosity.

Using then available data, Hodson & Zhao (2017) suggested that DF44 poses a problem for MOND, leading them to seek further modifications to the theory. The deep-MOND dynamical mass $\propto \sigma_{\rm los}^4$, meaning that underestimated measurement errors on $\sigma_{\rm los}$ can lead one to prematurely conclude against this highly nonlinear theory.

Bílek et al. (2019) revisited the question of whether MOND can adequately explain the internal kinematics of DF44, taking into account the latest $\sigma_{\rm los}$ measurements. Assuming isotropy of the velocity dispersion tensor and $M_{\rm dyn}/L_I = 1.3$, they found that MOND matches the observed $\sigma_{\rm los}$ in the central regions. The agreement is poorer in the outer regions, but the MOND prediction is still within 2σ of the observations.

We use spatially resolved stellar kinematic data of DF44 to test MOND and MOG by solving the Jeans equation and determining the expected $\sigma_{\rm los}$ profile. Since its stars experience an orbital acceleration $<a_0$, there will be clear water between the Newtonian and Milgromian predictions. We will show that the dynamics of DF44 can be explained in the MOND alternative to dark matter using an acceptable stellar M/L_I ratio without making further ad hoc modifications to MOND. The difference between our conclusions and those of Hodson & Zhao (2017) arise mainly from a subsequent downwards revision to $\sigma_{\rm los}$ (van Dokkum et al. 2019b).

Throughout this contribution we differentiate between the dynamical and stellar it M/L in the photometric I–band, $M_{\rm dyn}/L_I$ and M_*/L_I, respectively, with the latter including stellar remnants. The gravity theory used to calculate $M_{\rm dyn}/L_I$ should be clear from the context. If Newtonian gravitation without dark matter were correct, then the Newtonian $M_{\rm dyn}/L_I = M/L_I$. If Newtonian gravitation with dark matter in the galaxy were to be correct, then $M_{\rm dyn}/L_I > M/L_I$. If MOND is correct (taking into account the EFE), then the MOND $M_{\rm dyn}/L_I = M_*/L_I$ always. These statements hold for the case that tidal effects are not important.

Our paper is organized as follows—based on photometry of DF44 and our understanding of stars, the SPS prediction for its M_*/L_I ratio is presented in Section 2. After briefly reviewing the basics of the MOND and MOG theories and introducing the Jeans equation (Section 3), we present our results (Section 4). We then discuss our results in Section 5 and present our conclusions in Section 6.

2. SPS Prediction for the $M_{*/LI}$ Ratio in the IGIMF Context

We begin by discussing our SPS models, which we use to provide a gravity model-independent expectation for the M_*/L_I ratio of DF44. With the correct gravity theory, this must be consistent with what we infer from our dynamical modeling (Section 4.2).

2.1. The Galaxy-wide IMF

The stellar M_*/L_I ratio depends on the age and metallicity of the stellar population and the stellar initial mass function (IMF), which in turn depends on the metallicity and star formation rate (SFR; Kroupa et al. 2013; Yan et al. 2017; Jeřábková et al. 2018; Zonoozi et al. 2019). In galactic environment studies, the stellar IMF is usually assumed to be invariant. But there are observational indications that the galaxy-wide IMF (gwIMF) may depend on the star formation environment (cloud density and metallicity), becoming top-heavy under extreme starburst conditions (Dabringhausen et al. 2009, 2010, 2012; Banerjee et al. 2012; Marks et al. 2012; Kroupa et al. 2013; Jeřábková et al. 2017; Kalari et al. 2018; Schneider et al. 2018). The data suggest that with increasing embedded cluster metallicity and decreasing density, the IMF becomes less top-heavy. Changes to the IMF have also been proposed to explain M_*/L ratios estimated through integrated light analysis of globular clusters (GCs) in M31, which show an inverse trend with metallicity (Zonoozi et al. 2016; Haghi et al. 2017). Another argument supporting a systematic variation of the IMF is the fraction of low-mass X-ray binaries in Virgo GCs and ultra compact dwarf galaxies (Dabringhausen et al. 2012).

To quantify the gwIMF, Kroupa & Weidner (2003) formulated the integrated galaxy IMF (IGIMF) theory by assuming that all stars form in embedded clusters (Lada & Lada 2003; Megeath et al. 2016) and adding the IMFs of all clusters which form in a star formation epoch. Based on the IGIMF theory, the gwIMF is top-light (deficit of massive stars) in low-mass galaxies because they are expected to have a low SFR (Úbeda et al. 2007; Lee et al. 2009; Yan et al. 2017; Watts et al. 2018). The gwIMF is predicted to be more top-heavy in massive galaxies with a high SFR, as is observed (Hoversten & Glazebrook 2008; Lee et al. 2009; Meurer et al. 2009; Habergham et al. 2010; Gunawardhana et al. 2011; Hopkins 2018; Zhang et al. 2018).

There are also competing models based on the stochasticity of a universal gwIMF for the deficiency of high-mass stars in low-density regions, as suggested by deep H_α observations of M83's outskirts (Koda et al. 2012). The stochastic models, however, face the challenge of needing to account for the systematic shift with increasing SFR of the observationally deduced gwIMF being top-light for dwarf disk and top-heavy for massive disk galaxies (Lee et al. 2009; Gunawardhana et al. 2011). Old, dormant galaxies also indicate significant gwIMF variations at the low-mass end—elliptical galaxies may be dominated by very-low-mass stars (van Dokkum & Conroy 2010, 2011; Conroy et al. 2017), while ultra-faint dwarf galaxies may have a deficit of low-mass stars when compared to the canonical stellar population (Geha et al. 2013; Gennaro et al. 2018). Here, we study the influence of the gwIMF and star formation history on the stellar M_*/L_I ratio of DF44.

2.2. The Expected M_*/L_I Ratio in the IGIMF Context

Based on the canonical gwIMF[4], the M_*/L_I ratio of a 10 Gyr old DF44-like galaxy is about 1 in solar units. Assuming a bottom-heavy or top-heavy gwIMF, the M_*/L_I ratio would

---

[4] The "canonical gwIMF" or "canonical IMF" is the standard invariant two-part power-law IMF with Salpeter index of $\alpha_2 = 2.3$ for stellar mass $m > 0.5 M_\odot$ and $\alpha_1 = 1.3$ for smaller stellar masses.

increase owing to the higher fraction of low-mass stars or stellar remnants, respectively.

Here, we use the IGIMF theory to determine DF44's M_*/L_I ratio. In the IGIMF context, the gwIMF would be top-heavy if the SFR $> 1 M_\odot$ yr^{-1} (Yan et al. 2017; Jeřábková et al. 2018). We assume a constant galaxy-wide SFR over the duration of star formation, Δt. Assuming an age of 10 Gyr for DF44 (van Dokkum et al. 2019b), we calculate its M_*/L_I ratio for different values of its total mass and Δt. The SFR increases with decreasing Δt, because SFR $= M_{\rm tot}/\Delta t$, where $M_{\rm tot}$ is the total mass of all stars were formed in the galaxy.

Figure 1 shows the calculated present-day M_*/L_I ratio versus the total I-band luminosity for different Δt. The total luminosity of DF44 is $(3.0 \pm 0.6) \times 10^8 L_{I\odot}$, which we show as vertical lines. The bottom panel of Figure 1 shows the M_*/L_I ratio as a function of the star formation timescale Δt. Decreasing Δt leads to a higher present-day M_*/L_I ratio. This is because decreasing Δt increases the SFR which, in the context of the IGIMF, implies a more top-heavy IMF and hence a higher M/L as well as a higher average stellar age. Assuming that $\Delta t > 30$ Myr, the M_*/L_I ratio must be in the range of 1–4.

However, the expected M_*/L_I is almost independent of Δt for the canonical IMF because the galaxy is much older than Δt in the range considered (red line in Figure 1). The minor decrease of the expected M_*/L_I for the canonical IMF at $\Delta t \geqslant 2$ Gyr is due to the lower number of remnants formed for a longer duration of star formation.

3. Modeling the Velocity Dispersion in MOG and MOND

3.1. Modified Gravity

In the weak field approximation, one can obtain the exact static spherically symmetric solution of the MOG field equation for a point-like mass by perturbing the fields around Minkowski spacetime for an arbitrary distribution of non-relativistic matter (Moffat & Rahvar 2013). In this regime, the MOG gravitational potential $\Phi(\boldsymbol{x})$ and gravitational acceleration $a(\boldsymbol{x}) = -\boldsymbol{\nabla}\Phi(\boldsymbol{x})$ are found using the principle of super-position as follows (see their Equation (32)):

$$\Phi(\boldsymbol{x}) = -G\left[\int \frac{\rho(\boldsymbol{x}')}{|\boldsymbol{x} - \boldsymbol{x}'|}(1 + \alpha - \alpha e^{-\mu|\boldsymbol{x}-\boldsymbol{x}'|})d^3x'\right]. \quad (1)$$

Here, G is the Newtonian gravitational constant, α is determined by the coupling strength of the fifth force vector, Φ_μ, to the baryonic matter and μ is the range of this force. The parameters α and μ are the free parameters of the theory that should be universal parameters fixed by observations (Moffat & Toth 2009). The resulting MOG acceleration from a point-like mass M in the weak field regime contains a Yukawa-type force added to the Newtonian acceleration (Moffat 2006):

$$a_{\rm MOG}(\boldsymbol{r}) = \frac{GM}{r^2}\{1 + \alpha[1 - e^{-\mu r}(1 + \mu r)]\}. \quad (2)$$

The gravitational potential/field of an extended self-gravitating spherically symmetric system in MOG has been derived based on the point mass potential (Moffat & Rahvar 2013; Roshan & Abbassi 2014).

By rotation curve analysis of the THe HI Nearby Galaxy Survey (THINGS) catalog of galaxies with a wide range of luminosities (from $L_B = 7 \times 10^7 - 5 \times 10^{10} L_{B\odot}$), Moffat & Rahvar (2013) have shown that α and μ are universal
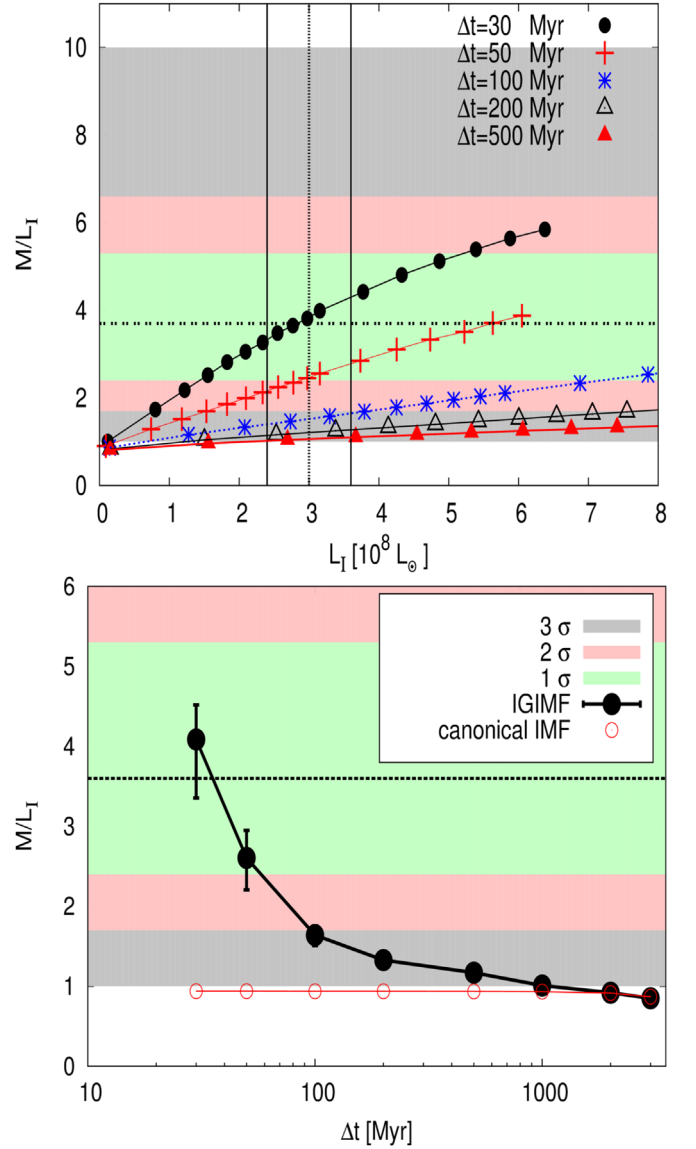
Figure 1. Top: M_*/L_I vs. the total I-band luminosity of a dwarf galaxy in the IGIMF context for different star formation durations of $\Delta t = 30, 50, 100, 200,$ and 500 Myr. The observed DF44 luminosity of $3 \times 10^8 L_{I\odot}$ is indicated by a vertical dotted line, with 20% lower and higher values shown with solid vertical lines to its left and right, respectively (Section 6.2 of van Dokkum et al. 2019b). The green, pink, and gray horizontal bands show the 1σ, 2σ, and 3σ ranges, respectively, of the inferred $M_{\rm dyn}/L_I$ in MOND, with the best-fitting value of 3.6 shown as a dotted line (Figure 2). Bottom: M_*/L_I ratio as a function of the star formation timescale Δt for the observed L_I of DF44 $\pm$ its 1σ uncertainty, obtained by interpolation in L_I for the IGIMF (black circles) and invariant canonical (red circles) gwIMF. In the latter case, the error bars are smaller than the points—this is also true for the IGIMF when $\Delta t \gtrsim 0.2$ Gyr. We also ran the 1 Gyr and 3 Gyr models with an exponential SFH, but do not show the results as M_*/L_I differs by $\lesssim 0.05$ from the corresponding model with a constant SFH.

parameters with the values $\alpha_{\rm RC} = 13$ and $\mu_{\rm RC} = 0.15 {\rm kpc}^{-1}$, respectively. They then applied the effective MOG potential with these fixed universal parameters to a sample of spiral galaxies in the Ursa Major catalog of galaxies and obtained good fits to galaxy rotation curve data. However, Haghi & Amiri (2016) showed that for almost all dSphs of the MW, the best-fitting values of α and μ are larger than $\alpha_{\rm RC}$ and $\mu_{\rm RC}$. They concluded that these parameters are not really universal constants in MOG as theoretically predicted (Green et al.

2018), but instead take different values for different classes of objects. In Section 4.3, we will confirm this conclusion again by showing that MOG with the universal parameters $\alpha_{\rm RC}$ and $\mu_{\rm RC}$ requires an unacceptable $M_{\rm dyn}/L_I$ ratio for DF44.

Since the total luminosity of DF44 ($L_I = 3 \times 10^8 L_{I\odot}$) is well within the luminosity range of the dwarf galaxies in their sample, in model MOG1 (see Section 4), we fix the MOG parameters to the upper limits obtained from the RC analysis of Moffat & Rahvar (2013).

3.2. Milgromian Dynamics

In the nonrelativistic version of MOND interpreted as modified gravity (comprehensively reviewed in Famaey & McGaugh 2012), the gravitational acceleration g in an isolated spherically symmetric system is related to the Newtonian gravity g_N by (Milgrom 1983a; Bekenstein & Milgrom 1984)

$$g_N = g\mu\left(\frac{g}{a_0}\right), \tag{3}$$

where Milgrom's constant $a_0 = 1.2 \times 10^{-10}\,{\rm m\,s^{-2}}$ is the transition acceleration of the theory below which Newtonian dynamics breaks down (Begeman et al. 1991; Famaey et al. 2007) and $\mu(x)$ is an interpolation function which is very close to x when $x \ll 1$ but saturates at 1 for $x \gg 1$. Different types of MOND interpolating functions have been used in the literature. The most common families of functions were reviewed in Famaey & McGaugh (2012). The transition around a_0 can be interpreted to be due to the quantum vacuum (Milgrom 1999; Smolin 2017; Cadoni & Tuveri 2019).

As the internal acceleration of DF44 is significantly below a_0, the choice of interpolation function has a negligible effect on our results. Here, we use the standard function $\mu(x) = x/\sqrt{1 + x^2}$. With this function, the MOND acceleration g is related to the Newtonian acceleration g_N as follows (Milgrom 1983b):

$$g = g_N\sqrt{\frac{1}{2} + \frac{1}{2}\sqrt{1 + 4\left(\frac{a_0}{g_N}\right)^2}}, \tag{4}$$

where $g_N \equiv GM/r^2$ at some 3D radius r within which the enclosed baryonic mass $M(r) = L_I(r) \times M/L_I$. This is determined by combining photometric observations of L_I with the chosen or fitted stellar M/L M/L_I.

To assess how DF44 should behave in MOND, we can apply the deep-MOND virial relation (Milgrom 1995) to estimate that its globally averaged one-dimensional velocity dispersion should be $\sqrt[4]{4GMa_0/81} = 22\,{\rm km\,s^{-1}}$ for an I-band luminosity of $3 \times 10^8 L_{I\odot}$ (van Dokkum et al. 2019b) and a stellar mass to light ratio of 1 solar unit in this band (Section 2). This is rather similar to their reported velocity dispersions, suggesting that MOND may be consistent with DF44.

3.3. Jeans Analysis

In order to find $\sigma_{\rm los}$ in a nonrotating spherically symmetric system, we use the Jeans equation (Binney & Tremaine 2008):

$$\frac{d(\nu(r)\sigma_r^2(r))}{dr} + \frac{2\nu(r)}{r}\beta(r)\sigma_r^2(r) = -\nu(r)\frac{d\Phi}{dr}, \tag{5}$$

Table 1
The Results of Fitting MOND and MOG Models to the Observational Line-of-sight Velocity Dispersion Profile, Which We Extracted from van Dokkum et al. (2019b)

Model	$M_{\rm dyn}/L_I$	β	α	μ (kpc^{-1})	χ_N^2 (P-value)
MOG 1	$7.4^{+1.5}_{-1.4}$	$-0.1^{+0.2}_{-0.4}$	13 (fixed)	0.15 (fixed)	0.43(0.15)
MOG 2	3 (fixed)	$0.0^{+0.20}_{-0.25}$	94^{+20}_{-19}	$0.09^{+0.01}_{-0.01}$	0.47(0.25)
MOG 3	1 (fixed)	$0.0^{+0.20}_{-0.25}$	109^{+21}_{-20}	$0.18^{+0.02}_{-0.03}$	0.52(0.29)
MOND	$3.6^{+1.6}_{-1.2}$	$-0.5^{+0.4}_{-1.6}$	...	...	0.58(0.25)

where r, $\nu(r)$, $\beta(r)$, $\sigma_r(r)$, and $\Phi(r)$ are the radial distance from the center of the galaxy, the spatial number density of stars, the velocity anisotropy, the radial velocity dispersion as a function of radial distance and the gravitational potential, respectively. In general, β could be zero (i.e., isotropic velocity dispersion tensor), constant, or a function of r.

The observable $\sigma_{\rm los}$ is given by

$$\sigma_{\rm los}^2(R) = \frac{\int_0^\infty [y^2 + (1 - \beta(r))R^2]r^{-2}\sigma_r^2(y)\nu(y)\,dy}{\int_0^\infty \nu(y)\,dy}, \tag{6}$$

where R and r are the 2D and 3D distances from the center of the galaxy, respectively, and $y \equiv \sqrt{r^2 - R^2}$.

For the density distribution, we use a Plummer model (Plummer 1911):

$$\nu(r) = \left(\frac{3M}{4\pi a_p^3}\right)\left(1 + \frac{r^2}{a_p^2}\right)^{-\frac{5}{2}}, \tag{7}$$

where M is the total mass of the galaxy and a_p is its Plummer radius, which is $\approx 1.3\times$ smaller than the 3D half-light radius r_h (Wolf et al. 2010). In this study, we assume $r_h = 3.5$ kpc and a total luminosity of $L_I = 3 \times 10^8 L_{I\odot}$ (van Dokkum et al. 2016, 2019b).

4. Results

By adjusting the free parameters of a model, the fit to the data can be improved or worsened. We quantify the goodness of each fit using the reduced χ^2 statistic, which is defined as

$$\chi_N^2 = \frac{1}{(N - P)}\sum_{i=1}^N \frac{(\sigma_{\rm los,theory}^i - \sigma_{\rm los,obs}^i)^2}{\sigma_i^2}, \tag{8}$$

where σ_i is the uncertainty of the observed data point i, $N = 9$ is the number of data points, and P is the number of degrees of freedom in the model.

4.1. MOG Fits

By applying the formalism described in Section 3 to the observed data of DF44, we calculate its $\sigma_{\rm los}$ profile. Given that DF44 has $L_I = 3 \times 10^8 L_{I\odot}$, its baryonic mass is within the range of galaxies in the THINGS catalog. Thus, in the first step (MOG1), we fix the MOG parameters to $\alpha_{\rm RC} = 13$ and $\mu_{\rm RC} = 0.15\,{\rm kpc^{-1}}$, which are upper limits inferred from fitting MOG to galaxy RCs (Moffat & Rahvar 2013).

We allow variation in the $M_{\rm dyn}/L_I$ ratio and anisotropy parameter β. As shown in Table 1, although a good fit is achieved with reduced $\chi^2 = 0.43$, the inferred $M_{\rm dyn}/L_I$ of
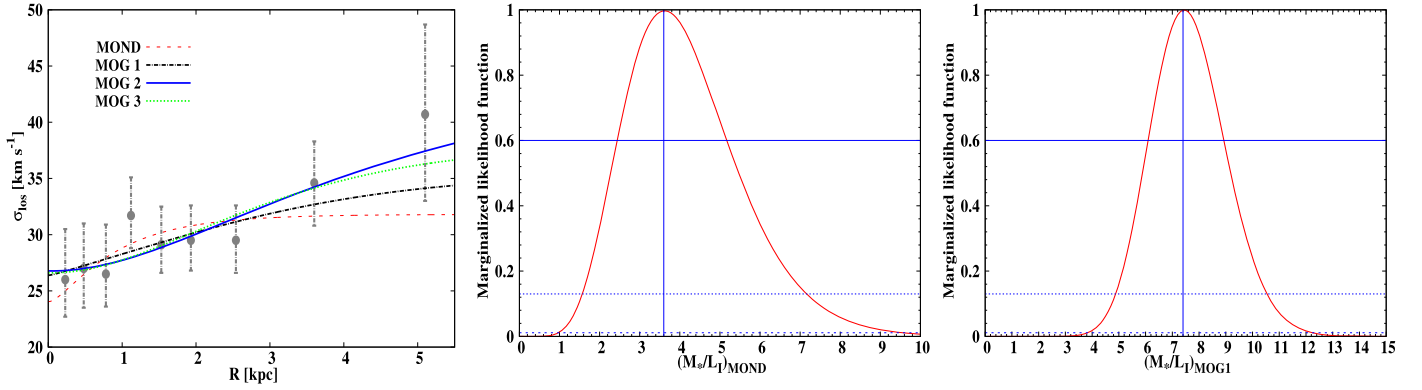
Figure 2. Left: the best fits to the DF44 $\sigma_{\mathrm{los}}(R)$ profile (van Dokkum et al. 2019b) obtained from the Jeans equation in MOND and MOG models. The *x*-axis is the sky-projected distance. Middle: the marginalized 68% (solid line), 95% (dotted line), and 99% (dashed line) confidence levels on M_{dyn}/L_I for the MOND model. Right: same as the middle panel but for the MOG1 model.

$7.4^{+1.5}_{-1.4}$ for model MOG1 is larger than expected from SPS models (Figure 2). We also derive the uncertainty on the M_{dyn}/L_I ratio. The marginalized 1σ, 2σ, and 3σ confidence intervals on M_{dyn}/L_I are indicated in the right-hand panel of Figure 2 as horizontal lines.

In order to produce higher values of σ_{los} with a lower M_{dyn}/L_I, one needs to assign larger values of α and μ compared to α_{RC} and μ_{RC}. Given that the above α_{RC} and μ_{RC} are upper limits, we conclude that the best-fitting parameters are inconsistent with limits imposed by rotation curve analyses. Indeed, it has already been shown that these parameters should not be taken as universal constants but should be considered as mass-dependent (Moffat 2006; Haghi & Rahvar 2010; Haghi & Amiri 2016). For example, fits to σ_{los} data of the MW dSph galaxies yield average values of $\alpha_{\mathrm{dSph}} = 221 \pm 112$ and $\mu_{\mathrm{dSph}} = 0.41 \pm 0.35 \ \mathrm{kpc}^{-1}$ (Haghi & Amiri 2016).

Therefore, in the second step, we let these two parameters vary and fit the velocity dispersion data with a fixed $M/L_I = 3$ (model MOG2) or 1 (model MOG3) solar units. Figure 2 shows that the MOG theory can successfully reproduce the observed data with acceptable values of χ^2. In these cases, MOG prefers an isotropic velocity dispersion tensor of DF44 (i.e., $\beta \approx 0$).

As shown in Table 1, the best-fitting values of $94 \leqslant \alpha \leqslant 109$ and $0.09 \leqslant \mu \leqslant 0.18 \ \mathrm{kpc}^{-1}$ are consistent with the results for dSph galaxies (Haghi & Amiri 2016). However, the best-fitting α values are larger than those inferred from rotation curve analysis of spiral galaxies, supporting the hypothesis that the MOG parameters are mass-dependent. This is consistent with the trend claimed by Brownstein & Moffat (2007) that the best-fitting values of α and μ decrease when moving from low-mass systems (e.g., dwarf galaxies) to massive systems (e.g., dwarf and normal X-ray clusters). However, MOG does not offer a physical explanation for such a dependency.

4.2. MOND Fit

By solving the Jeans equation, we calculate $\sigma_{\mathrm{los}}(R)$ in the MOND framework. The best-fitting values of the *M/L* and anisotropy parameter along with the minimum χ^2 value are given in Table 1. The MOND fit to the σ_{los} profile is shown in Figure 2 as a red dashed line. The reduced χ^2 of 0.58 is quite good, as can also be seen in Figure 2—the best-fitting profile passes through eight out of nine data points within their 1σ uncertainties, while the prediction for the outermost point is

only just outside its 1σ range. In this model, the anisotropy is negative ($\beta = -0.5$), i.e., the tangential velocity dispersion exceeds the radial one. In addition, to be comfortably explained in MOND, DF44 should have a M_{dyn}/L_I ratio of around 3.6 solar units. Our result is in good agreement with those of Bílek et al. (2019), who found the tangentially anisotropic model with $\beta = -0.5$ and $M_{\mathrm{dyn}}/L_I = 3.9$ provides a reasonable fit to the data (see their Figure 2b).

As can be seen in Figure 2, the M_{dyn}/L_I ratio of $3.6^{+1.6}_{-1.2}$ inferred from our MOND dynamical model of DF44 (shown as horizontal lines) can be acceptable in the context of the IGIMF theory if the star formation occurred very rapidly (within the first 50–80 Myr) and shut off thereafter (Figure 1).

At 3σ, our MOND dynamical modeling is consistent with $M_*/L_I = 1.0$ (middle panel of Figure 2). The significant uncertainty in this is a consequence of the fact that $\sigma \propto \sqrt[4]{M}$ in the deep-MOND limit, allowing large changes in M_*/L_I to have a relatively modest impact on the observed kinematics. A M/L of $M_*/L_I = 1.0$ arises in our IGIMF model for $\Delta t = 1$ Gyr (Figure 1). This is longer than DF44's dynamical timescale of $t_{\mathrm{dyn}} = r_h/\sigma \approx 66$ Myr if $r_h = 3.5$ kpc and the 3D velocity dispersion σ is $\sqrt{3} \times$ the observed σ_{los} of 30 km s^{-1}.

A short star formation timescale, being consistent with MOND, might also naturally explain the large size of DF44, since gas expelled by massive stars would cause it to expand (Wu & Kroupa 2018). This result is in line with the suggestion by van Dokkum et al. (2018) that UDGs must have had extremely high gas densities at the time of their formation and perhaps feedback from an intense, compact starburst that created them caused both the cessation of star formation and their expansion to become UDGs.

In the context of the IGIMF theory, the slope of the gwIMF above 1 $M_\odot$ varies with the SFR. A higher SFR leads to the gwIMF being more top-heavy, while the slope of the gwIMF does not change for $m < 1 M_\odot$ and remains the same as the canonical IMF (but see Jeřábková et al. 2018). Adopting an age of 10 Gyr and $\Delta t < 500$ Myr, only stars with $m < 1 M_\odot$ remain alive on the main sequence and contribute to the total luminosity. Stars with higher masses have already evolved and turned into remnants, so they contribute to the total mass but not to the luminosity. Since we fix the *I*-band luminosity of the modeled galaxies to be the same as DF44, adopting the IGIMF instead of the canonical IMF only changes the total mass of DF44 and hence its M_*/L_I. DF44's suggested short
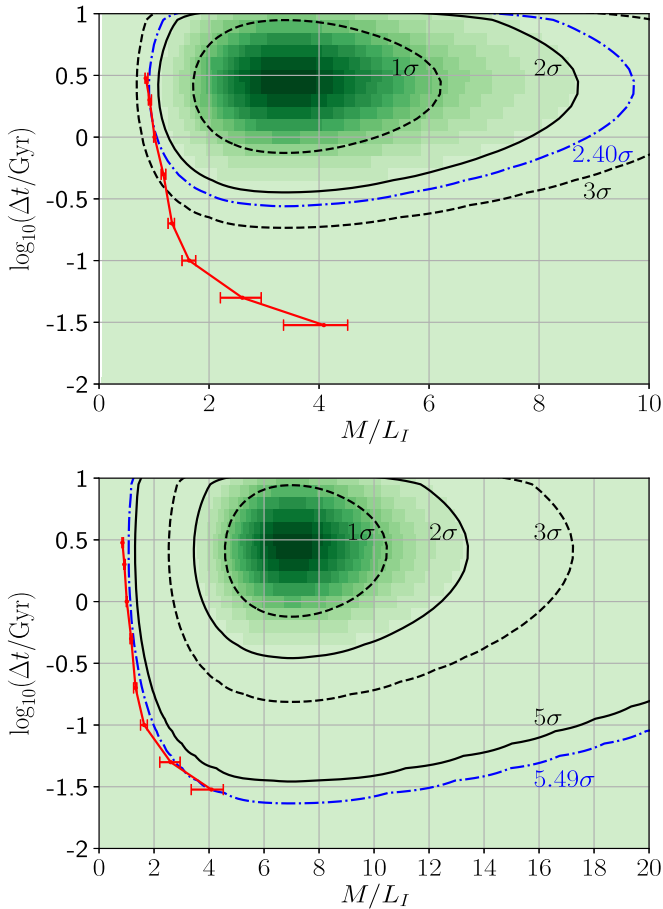
Figure 3. Indicated contours of the joint probability of the stellar $M_{\rm dyn}/L_I$ ratio and $\log_{10}(\Delta t/{\rm Gyr})$ for MOND (top panel) and MOG1 (bottom panel), calculated with Equation (9). In both panels, the red tracks are M_*/L_I values of our SPS models in the IGIMF framework for $L_I = (3.0 \pm 0.6) \times 10^8 L_{I\odot}$ (Section 1) while the blue contours marginally intersect a point on these tracks.

star formation duration implies that its color will be independent of Δt as long as this is much less than its age.

4.3. Consistency with Observations

In this section, we show the joint constraint on the M/L_I and Δt of DF44 based on dynamical modeling and typical values of Δt as found by Pflamm-Altenburg & Kroupa (2009), respectively. We also show the locus of $(M/L_I, \Delta t)$ values consistent with stellar population modeling in the IGIMF framework (Section 2).

We begin by plotting a 2D array of probabilities as a function of $M_{\rm dyn}/L_I$ and $\log_{10}(\Delta t)$ (with Δt in Gyr). We then show the 68.3%, 95.4%, and 99.7% confidence levels of the probability distribution (Figure 3). The probability P is the product of the posterior on $M_{\rm dyn}/L_I$ from the kinematics (Equation (8)) multiplied by the likelihood of a particular star formation timescale, i.e.,

$$P(M_{\rm dyn}/L_I, \Delta t) = P(M_{\rm dyn}/L_I) \times P(\Delta t), \text{ where}$$

$$P(\Delta t) \propto \exp\left(-\frac{(\log_{10}\Delta t - \log_{10}\Delta t_{\rm expected})^2}{2\sigma^2}\right) \quad (9)$$

and $\Delta t_{\rm expected} = 2.9\,{\rm Gyr}$ is the expected Δt from Pflamm-Altenburg & Kroupa (2009) for an assumed gas mass of $10^6 M_\odot$ (using a $10\times$ lower or higher value has a negligible effect).

According to Section 5 of their work, Δt has a dispersion of $\sigma = 0.36$ dex. We impose an upper limit of $\Delta t \leqslant 10$ Gyr because the red color of DF44 shows it did not form stars very recently. Since our dynamically inferred posteriors on $M_{\rm dyn}/L_I$ (Figure 2) are calculated for fixed $L_I = 3 \times 10^8 L_{I\odot}$, we convolve our $P(M/L_I)$ with a Gaussian in $\log_{10}(L_I)$ of width $0.088 = \frac{1}{2}(\log_{10}(1.2) - \log_{10}(0.8))$, thereby accounting for a 20% uncertainty in L_I (Section 6.2 of van Dokkum et al. 2019b).

To quantify the consistency of each model with observations, we change the confidence level until the corresponding contour just intersects one point on the SPS track of $(M_*/L_I, \Delta t)$. In this way, we find that MOND is consistent with observations at 1.66%, which corresponds to 2.40σ for a Gaussian distribution. However, MOG1 is consistent with observations only at the 4.07×10^{-8} level (5.49σ), so our results rule out MOG in its present form—we are already setting its free parameters to the upper limits allowed by THINGS (Section 4.1).

The MOND model marginally matches the data if we bear in mind that there must occasionally be 3σ outliers from the correct theory. Given that we have accurate kinematics for ≈ 200 galaxies and MOND works well in the vast majority of them (Li et al. 2018), we expect to come across a few cases where the consistency is only at the percent level. Indeed, it would be somewhat unusual if MOND explained all observed galaxies within 2.4σ. However, there should be no 5.5σ events within a sample of this size, showing that presently available data on DF44 rule out the MOG model if its free parameters are universal (as claimed by its proponents; Green et al. 2018) and our other modeling assumptions are correct. If DF44 has some rotation within the plane of the sky, its self-gravity would be even stronger than we assumed, thus requiring an even larger $M_{\rm dyn}/L_I$ and making the situation worse for MOG. The same is true if we use the canonical IMF instead of the IGIMF as the former predicts $M_*/L_I = 1$ (Figure 1).

5. Discussion

van Dokkum et al. (2019b) recently reported a revised stellar velocity dispersion within the effective radius for the UDG known as DF44, implying its Newtonian $M_{\rm dyn}/L_I \approx 26$ solar units. They argue that the galaxy is gravitationally dominated by dark matter, in apparent contrast to the UDGs DF2 and DF4. They claimed that the MOND-predicted velocity dispersion of DF44 is lower than the observed value, challenging alternatives to dark matter theories such as MOND.

We took DF44 to be in equilibrium by adopting a simplified density profile without any tidal interaction. Tidal disruption scenarios cannot easily be reconciled with the high GC counts of UDGs in Coma and their lack of obvious tidal features. The fact that DF44 appears to live in a dynamically cold environment (van Dokkum et al. 2019b, their Section 6.1) can be interpreted as evidence against tidal heating by the Coma cluster. However, some tidal heating could increase the velocity dispersion in the outer parts of DF44, easing the tension with MOND (Bílek et al. 2019).

In addition to neglecting tides, our MOND calculations assume no EFE (see Famaey & McGaugh 2012 for a review and discussion of the MOND-unique EFE; see also Wu & Kroupa (2015) for an accessible description). Since the internal acceleration is $g_{\rm int} \approx \sqrt{GMa_0}/r_h = 0.24\,a_0$ for $M_*/L_I = 1$,

the EFE would not significantly affect our results as long as the external field (EF) is much weaker than this. The MOND dynamical mass of the Coma cluster is $4.6 \times 10^{14} M_\odot$ (Sanders 2003). This implies that DF44 is $\gg 3.0$ Mpc from the center of the Coma cluster, in which case DF44 is not in the cluster. This is entirely consistent with its sky-projected separation of ≈ 1.7 Mpc (Bílek et al. 2019, their Section 3.1) and the observation that two other galaxies, DF42 and DFX2, have a radial velocity within $100 \, \mathrm{km \, s^{-1}}$ of the value for DF44, suggesting these are part of a different group which is dynamically much colder than the Coma cluster (van Dokkum et al. 2019b, their Section 6.1). For an MW-like galaxy with $M = 10^{11} M_\odot$ to provide an EF comparable to g_int, the separation with DF44 would need to be $\lesssim 24$ kpc. There is no such galaxy so close to DF44, strengthening confidence in our assumption that it can be treated as isolated.

So far, we have assumed that DF44 is at a downrange distance of $D = 100$ Mpc based on its redshift. However, it may have a peculiar velocity of a few hundred $\mathrm{km \, s^{-1}}$. The MOND-predicted $\sigma_\mathrm{los} \propto \sqrt{D}$ for fixed M/L_I and apparent magnitude (Kroupa et al. 2018). Since $\sigma_\mathrm{los} \propto \sqrt[4]{M}$ in the deep-MOND limit (Milgrom 1995), the MOND $M_\mathrm{dyn}/L_I \propto D^{-2}$. Thus, placing DF44 just 10% further away reduces the best-fitting M_dyn/L_I to 3.0, improving the agreement with SPS expectations. Its observed velocity dispersion could also have been overestimated slightly.

Our analysis prefers a relatively short formation timescale for DF44. This can occur if it is a tidal dwarf galaxy and lost its gas reservoir by ram pressure or tidal stripping, i.e., if it was quenched (Weisz et al. 2015). The temporal evolution of the quenched fraction can also provide clues as to how quickly dwarf galaxies can undergo quenching. For example, in the lowest-mass systems, nearly 40% already appear to be quenched by ≈ 12 Gyr ago, which implies a quenching timescale of 1–2 Gyr (Weisz et al. 2015). Therefore, DF44 may well have been quenched within 1 Gyr of its formation.

Once there is no further gas supply, the available gas is consumed on a dynamical timescale. Pressure supported systems do indeed form within a few dynamical times, as is nicely evident in elliptical galaxies—see the downsizing results by Thomas et al. (1999) and Recchi et al. (2009). Since DF44 is pressure supported (van Dokkum et al. 2016), it may well have a somewhat shorter Δt than estimated by Pflamm-Altenburg & Kroupa (2009) because their work only considered late-type galaxies.

6. Conclusion

We constructed SPS models of DF44 in the IGIMF framework to estimate its stellar M_*/L_I ratio independently of the assumed gravity law. We then used spatially resolved kinematic data of DF44 to infer its dynamical M_dyn/L_I in the framework of MOG and MOND, which are alternative approaches to the cold dark matter hypothesis. The main conclusions of these calculations are as follows:

1. First, we used MOG with the upper limits $\alpha_\mathrm{RC} = 13$ and $\mu_\mathrm{RC} = 0.15 \mathrm{kpc}^{-1}$ inferred from fits to galaxy rotation curves (Moffat & Rahvar 2013). The only free parameter was the stellar M_*/L_I ratio. We found that these models provide a reasonably good fit, but the required high near-infrared M_dyn/L_I ratio of ≈ 7.4 solar units is completely inconsistent with SPS modeling for any plausible star formation duration.

2. Then, we let α and μ vary as free parameters and fitted the velocity dispersion data assuming $M_*/L_I = 1$ and 3 solar units. The best-fitting values of α and μ are larger than α_RC and μ_RC, supporting the hypothesis that the MOG parameters are mass-dependent. They are compatible with the average values of $\alpha = 221 \pm 112$ and $\mu = 0.41 \pm 0.35 \mathrm{kpc}^{-1}$ obtained from fitting MOG to σ_los data of the MW dSph galaxies (Haghi & Amiri 2016). These values are significantly larger than α_RC and μ_RC inferred from fits to the rotation curves of spiral galaxies (Moffat & Rahvar 2013).

3. We calculated the σ_los profile of DF44 in MOND and found that the best-fitting model with constant orbital anisotropy has $\beta = -0.5^{+0.4}_{-1.6}$ and a stellar M/L of $M_\mathrm{dyn}/L_I = 3.6^{+1.6}_{-1.2}$ solar units. Obtaining $M_*/L_I = 3.6$ requires a star formation duration $\Delta t \approx 40$ Myr. However, the 3σ lower limit on M_dyn/L_I is 1.0, consistent with the canonical IMF and expectations from SPS modeling in the IGIMF context for $\Delta t < 1$ Gyr (Figure 1).

4. By considering the joint constraints on M/L_I and Δt from dynamical modeling and observations of other galaxies, respectively, we showed that MOND is consistent with our $\Delta t = 2$ Gyr star formation model of DF44 at 2.40σ (1.66% confidence). The same approach shows that MOG is ruled out at 5.49σ because it has only a 4.07×10^{-8} chance of explaining the observations even if α and μ are set to the upper limits inferred from rotation curve fitting.

ORCID iDs

Hosein Haghi ⓘ https://orcid.org/0000-0002-9058-9677
Akram Hasani Zonoozi ⓘ https://orcid.org/0000-0002-0322-9957
Indranil Banik ⓘ https://orcid.org/0000-0002-4123-7325
Pavel Kroupa ⓘ https://orcid.org/0000-0002-7301-3377

References

Angus, G. W., & McGaugh, S. S. 2008, MNRAS, 383, 417
Banerjee, S., Kroupa, P., & Oh, S. 2012, MNRAS, 426, 1416
Begeman, K. G., Broeils, A. H., & Sanders, R. H. 1991, MNRAS, 249, 523
Bekenstein, J., & Milgrom, M. 1984, ApJ, 286, 7
Bílek, M., Müller, O., & Famaey, B. 2019, A&A, 627, L1
Binney, J., & Tremaine, S. 2008, Galactic Dynamics (2nd ed.; Princeton, NJ: Princeton Univ. Press)
Brownstein, J. R., & Moffat, J. W. 2007, MNRAS, 382, 29
Cadoni, M., & Tuveri, M. 2019, PhRvD, 100, 024029
Conroy, C., van Dokkum, P. G., & Villaume, A. 2017, ApJ, 837, 166
Dabringhausen, J., Fellhauer, M., & Kroupa, P. 2010, MNRAS, 403, 1054
Dabringhausen, J., Kroupa, P., & Baumgardt, H. 2009, MNRAS, 394, 1529
Dabringhausen, J., Kroupa, P., Pflamm-Altenburg, J., & Mieske, S. 2012, ApJ, 747, 72
Danieli, S., van Dokkum, P., Conroy, C., Abraham, R., & Romanowsky, A. J. 2019, ApJL, 874, L12
Di Cintio, A., Brook, C. B., Dutton, A. A., et al. 2017, MNRAS, 466, L1
Di Cintio, A., Brook, C. B., Dutton, A. A., et al. 2014, MNRAS, 441, 2986
Famaey, B., Bruneton, J.-P., & Zhao, H. 2007, MNRAS, 377, L79
Famaey, B., McGaugh, S., & Milgrom, M. 2018, MNRAS, 480, 473
Famaey, B., & McGaugh, S. S. 2012, LRR, 15, 10
Geha, M., Brown, T. M., Tumlinson, J., et al. 2013, ApJ, 771, 29

Gennaro, M., Tchernyshyov, K., Brown, T. M., et al. 2018, ApJ, 855, 20
Green, M. A., Moffat, J. W., & Toth, V. T. 2018, PhLB, 780, 300
Gunawardhana, M. L. P., Hopkins, A. M., Sharp, R. G., et al. 2011, MNRAS, 415, 1647
Habergham, S. M., Anderson, J. P., & James, P. A. 2010, ApJ, 717, 342
Haghi, H., & Amiri, V. 2016, MNRAS, 463, 1944
Haghi, H., Khalaj, P., Hasani Zonoozi, A., & Kroupa, P. 2017, ApJ, 839, 60
Haghi, H., & Rahvar, S. 2010, IJTP, 49, 1004
Haghi, H., Kroupa, P., Banik, I., et al. 2019, MNRAS, 487, 2441
Hodson, A. O., & Zhao, H. 2017, A&A, 607, A109
Hopkins, A. M. 2018, PASA, 35, 39
Hoversten, E. A., & Glazebrook, K. 2008, ApJ, 675, 163
Jeřábková, T., Hasani Zonoozi, A., Kroupa, P., et al. 2018, A&A, 620, A39
Jeřábková, T., Kroupa, P., Dabringhausen, J., Hilker, M., & Bekki, K. 2017, A&A, 608, A53
Kalari, V. M., Carraro, G., Evans, C. J., & Rubio, M. 2018, ApJ, 857, 132
Koda, J., Yagi, M., Boissier, S., et al. 2012, ApJ, 749, 20
Kroupa, P., & Weidner, C. 2003, ApJ, 598, 1076
Kroupa, P., Weidner, C., Pflamm-Altenburg, J., et al. 2013, in The Stellar and Sub-Stellar Initial Mass Function of Simple and Composite Populations, ed. T. D. Oswalt & G. Gilmore (Dordrecht: Springer), 115
Kroupa, P., Haghi, H., Javanmardi, B., et al. 2018, Natur, 561, E4
Lada, C. J., & Lada, E. A. 2003, ARA&A, 41, 57
Lee, J. C., Gil de Paz, A., Tremonti, C., et al. 2009, ApJ, 706, 599
Li, P., Lelli, F., McGaugh, S., & Schombert, J. 2018, A&A, 615, A3
Marks, M., Kroupa, P., Dabringhausen, J., & Pawlowski, M. S. 2012, MNRAS, 422, 2246
Megeath, S. T., Gutermuth, R., Muzerolle, J., et al. 2016, AJ, 151, 5
Meurer, G. R., Wong, O. I., Kim, J. H., et al. 2009, ApJ, 695, 765
Milgrom, M. 1983a, ApJ, 270, 365
Milgrom, M. 1983b, ApJ, 270, 371
Milgrom, M. 1995, ApJ, 455, 439
Milgrom, M. 1999, PhLA, 253, 273
Moffat, J. W. 2005, JCAP, 5, 003
Moffat, J. W. 2006, JCAP, 3, 4
Moffat, J. W., & Rahvar, S. 2013, MNRAS, 436, 1439
Moffat, J. W., & Toth, V. T. 2009, CQGra, 26, 085002
Pflamm-Altenburg, J., & Kroupa, P. 2009, ApJ, 706, 516
Plummer, H. C. 1911, MNRAS, 71, 460
Recchi, S., Calura, F., & Kroupa, P. 2009, A&A, 499, 711
Roshan, M., & Abbassi, S. 2014, PhRvD, 90, 044010
Sanders, R. H. 2003, MNRAS, 342, 901
Schneider, F. R. N., Sana, H., Evans, C. J., et al. 2018, Sci, 359, 69
Smolin, L. 2017, PhRvD, 96, 104042
Thomas, D., Greggio, L., & Bender, R. 1999, MNRAS, 302, 537
Úbeda, L., Maíz-Apellániz, J., & MacKenty, J. W. 2007, AJ, 133, 932
van Dokkum, P., Danieli, S., Abraham, R., Conroy, C., & Romanowsky, A. J. 2019a, ApJL, 874, L5
van Dokkum, P., Abraham, R., Brodie, J., et al. 2016, ApJL, 828, L6
van Dokkum, P., Cohen, Y., Danieli, S., et al. 2018, ApJL, 856, L30
van Dokkum, P., Wasserman, A., Danieli, S., et al. 2019b, ApJ, 880, 91
van Dokkum, P. G., Abraham, R., Merritt, A., et al. 2015, ApJL, 798, L45
van Dokkum, P. G., & Conroy, C. 2010, Natur, 468, 940
van Dokkum, P. G., & Conroy, C. 2011, ApJL, 735, L13
Wasserman, A., Romanowsky, A. J., Brodie, J., et al. 2018, ApJL, 863, L15
Watts, A. B., Meurer, G. R., Lagos, C. D. P., et al. 2018, MNRAS, 477, 5554
Weisz, D. R., Dolphin, A. E., Skillman, E. D., et al. 2015, ApJ, 804, 136
Wolf, J., Martinez, G. D., Bullock, J. S., et al. 2010, MNRAS, 406, 1220
Wu, X., & Kroupa, P. 2015, MNRAS, 446, 330
Wu, X., & Kroupa, P. 2018, ApJ, 853, 60
Yan, Z., Jerabkova, T., & Kroupa, P. 2017, A&A, 607, A126
Zhang, Z.-Y., Romano, D., Ivison, R. J., Papadopoulos, P. P., & Matteucci, F. 2018, Natur, 558, 260
Zonoozi, A. H., Haghi, H., & Kroupa, P. 2016, ApJ, 826, 89
Zonoozi, A. H., Mahani, H., & Kroupa, P. 2019, MNRAS, 483, 46